# Constellation Design for Cascaded *M*PSK-CSK Systems

A. R. Ndjiongue*, H. C. Ferreira* and Telex M. N. Ngatched⊛
* Department of Electrical and Electronic Engineering Science, University of Johannesburg,
P.O. Box 524, Auckland Park, 2006, Johannesburg, South Africa.
⊛ Faculty of Engineering and Applied Science, Memorial University,
St. John's, NL A1B 3X5, Canada.
Emails: {arrichard,hcferreira}@uj.ac.za,tngatched@grenfell.mun.ca

***Abstract*—This paper proposes a constellation design for color shift keying (CSK) based on phase shift keying (PSK) conversion, to be used in cascaded power line communications (PLC) and visible light communications (VLC) systems integration. We optimize the design of *M*PSK-CSK constellations and analyze the performance of *M*PSK-CSK systems based on the optimized Euclidean distance calculated on the red-green-blue (RGB) color space.**

***Index Terms*—*M*PSK-CSK constellation design, hybrid PLC-VLC systems, *M*PSK-CSK systems, cascaded channels, PLC-VLC interface. PSK and CSK schemes, RGB colors space.**

## I. Introduction

Visible light communications (VLC) and power line communications (PLC) present many similarities including that they are parts of the electrical power system and that they both represent a communication technology. Interfacing both technologies has become one of the major research fields in telecommunication engineering, owing firstly to the advantages provided by both technologies when taken individually (for example, ubiquitous power line infrastructure and power saving light emitting diodes (LEDs)), secondly to the physical link between the power wires and the light source. Added to these reasons, PLC technology could be used as return path in VLC duplex transmissions or VLC could be used to connect the PLC end user. Additionally, PLC technology is seen as the best backbone for VLC technology.

From the PLC standards point of view, IEEE 1901 [1]–[3], ITU-T G.9955/56, ITU-T G.9960/61 [4], G3-PLC, PRIME and HOMEPLUG, propose modulation techniques including orthogonal frequency division multiplexing (OFDM) with phase shift keying (PSK), quadrature amplitude modulation (QAM) or amplitude PSK (APSK) over sub-carriers. PSK is a digital modulation technique that convey information by changing the phase of the carrier signal. PSK is very solicited in transmission systems where the amplitude of the received signal cannot be trusted, even though it is weak against phase noise. Then, PSK provides the important advantage that the amplitude of the transmitted signal does not play a major role in symbol transmission. Even though PSK is weak against phase noise, this aspect is a vital key for the report proposed in this paper.

In VLC technology, the fast increasing number of research reports shows the interest of the research community in seeing a massive deployment of the technology. Color shift keying (CSK), proposed in IEEE 802.15.7 [5] and analyzed in [6]–[10], is a digital modulation technique exploiting color variation for data transmission. The information is concealed in a color produced using red-green-blue (RGB) LEDs. The constellation in CSK fits in a triangle that is compartmented to form decision regions. CSK could be the main modulation technique to be adapted in applications such as light fidelity (Li-Fi). This scheme presents numerous advantages when compared to other modulation techniques. For example, there is no inrush current and no flickering in CSK.

In color technology, many color spaces are available to be used. They are dedicated to specific applications. For example, the Cyan-Magenta-Yellow-Key (CMYK) color model is used in printing owing to its ease to directly producing the black color. In the same sense, the hue-saturation-value (HSV) is mostly used in image detection owing to its facility to extract color parameters (*i.e* saturation, chroma, value, hue) of an image. On the other side, the RGB color space is for example exploited in color television for its ease to produce the rest of colors by modulating the intensities of the currents flowing in the circuits. The CSK technique is based on producing colors by modulating the intensities of the currents flowing in the RGB-LEDs used. Conversion matrices are available to change color space, also, algorithms are available to convert the complex plane to a color space [11], [12]. The most used conversion algorithm between complex vectors and colors is based on the color wheel and uses the HSV color space [11], [12].

A great number of research reports focusing on interfacing PLC and VLC have been proposed, [13]–[21] to mention only few of them. They all propose solutions to make possible the integration of PLC and VLC technologies. We briefly present some of the work that has been done to add value in PLC-VLC integration. [13] is one of the precursors of PLC-VLC integration. It proposes a system exploiting PSK over the PLC channel and retransmitting over the VLC channel using white LEDs, without demodulating the signal from the power-line.

[14] proposes a novel and cost-effective indoor broadband broadcasting PLC-VLC integration while [15] focuses on applying hybrid broadband PLC-VLC systems based on OFDM modulation in hospital applications. In [16], the performance of cascaded PLC-VLC systems using OFDM and CSK is proposed. [17] reviews the state of both broadband PLC and VLC systems and proposes new directions for PLC-VLC integration. [18] applies a spatial-optical OFDM in PLC-VLC systems while [19] and [20] focus on practically implementing hybrid PLC-VLC systems based on spread frequency shift keying (SFSK) and on-off keying (OOK). In [21]–[23], a technique to map PSK symbols to colors using the color wheel and the HSV color space is proposed. It exploits the aforementioned knowledge of PSK modulation technique on the magnitude of the PSK symbol, to control transmission and lighting performances of hybrid PLC-VLC systems. In this technique, the amplitude of the *M*PSK (PLC) received symbol is altered to control both transmission and illumination over the VLC channel. Note that the technique proposed in [21]–[23], for which the constellation design is given here presents two important advantages which are: (*i*) Natural mapping between PSK and CSK implying very less processing between PLC and VLC channels (cascaded channels) and (*ii*) constant lighting provided by RGB-LEDs without using any other compensation circuit.

In this paper, we propose an optimal constellation design for such hybrid PLC-VLC systems. It is shown that the increment of *M*PSK-CSK constellation size is done at the expense of the communication performance. However, for all constellation sizes, a trade-off between communication and lighting is obtained by maximizing the product $V \times S$ of the value by the saturation or their average $0.5(V + S)$. We optimize the design of a *B*PSK-CSK constellation and apply the result to any *M*PSK-CSK constellation size. Note that the color rendering requirement and the VLC channel effect are not taken into account in this paper.

The remainder of the paper proposes a model of *M*PSK-CSK systems in Section II and gives a quick view of the background of the error probability computation in Section III. The optimized constellation design is proposed in Section IV. The Euclidean distance is analyzed and some results on analytical bit error rate (BER) are proposed. Finally, the paper is concluded in Section V.

## II. *M*PSK-CSK System Model

A model of *M*PSK-CSK interface is proposed in Fig. 1. The $j^{th}$ symbol $\mathbf{z}_j$ ($j = 0, 1, 2, \ldots, M-1$), detected over the PLC channel, essentially has a magnitude $|\mathbf{z}_j|$ and a phase $\theta_J$. The PSK demodulator does not pay attention to the value of $|\mathbf{z}_j|$. Later, we will use $|\mathbf{z}_j|$ to control lighting and transmission over the VLC channel. The algorithm used in the color wheel is based on the three following equations: $H_j = \arg(\mathbf{z}_j)$, $V_j = 0.5 + 0.5\cos(2\pi r_j)$ and $S_j = 0.5 + 0.5\sin(2\pi r_j)$. To do the mapping, the color wheel exploits the advantage that $\theta_j$ and $H_j$ are angles and vary between 0 and $\pi$. $V_j$ and $S_j$ are computed base on $r_j = 1 + \ln(1 + |\mathbf{z}_j|)$. Hence,

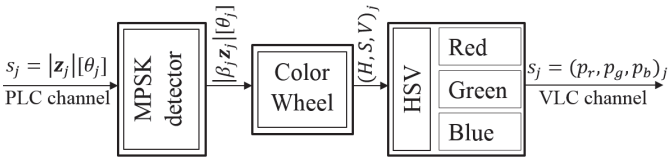


Figure 1. *M*PSK-CSK interface model showing only the blocks between PLC and VLC channels.

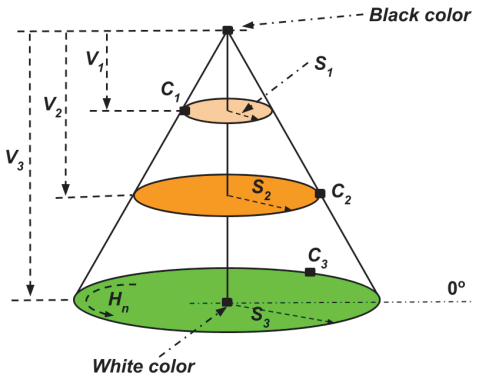


Figure 2. HSV color space represented by its half-cone.

they vary with $|\mathbf{z}_j|$. We then impose a factor $\varepsilon_j$ to modulate $V_j$ and $S_j$. $\varepsilon_j$ is an amplification factor used to repair all distortions that happened to $|\mathbf{z}_j|$ over the PLC channel, due to attenuation and noise. In the design optimization proposed in Section IV, we will show the variation of $V(\mathbf{x})$ and $S(\mathbf{x})$. We match the obtained ($H_j$,$S_j$,$V_j$) to an RGB color so that the transmission uses RGB-LEDs. Three currents are allocated to the RGB-LEDs to produce the color $\mathbf{c}_j$ corresponding to the complex symbol $\mathbf{z}_j$. Thus, the constellation of size *M* obtained is called *M*PSK-CSK constellation. It shares its size with the original PSK constellation and with the final CSK constellation. The transmission over the VLC channel must meet the lighting requirement $[(p_r + p_g + p_b)_j = 1]$ and the communication objectives (*i.e* maximizing the minimum Euclidean distance between the nearest colors in the sender constellation). The lighting requirement is permanently met and represents one specific advantage of the HSV color space: All colors situated at the same distance from the black color are produced with the same lighting intensity (value $V$ of HSV, see Fig. 2). Fig. 2 shows the HSV half-cone. Three values of the intensity ($V_1, V_2, V_3$) and saturation ($S_1, S_2, S_3$), and the rotation direction of $H$ are shown. The axis is $White-Black$, and gives the lighting level (values of $V$) and the radii of the plates correspond to saturation levels (values of $S$). We use $\varepsilon_j$ to voluntarily vary $V_j$ and $S_j$ when needed. $\varepsilon_j$ helps keeping the product $\varepsilon_j|\mathbf{z}_j|$ constant for all PSK symbols detected over the PLC channel. Then, the main aim of the constellation design proposed in this paper is to find the best trade-off between lighting and communication. We will then

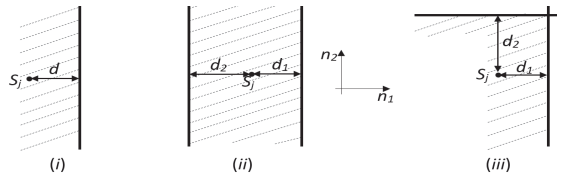


Figure 3. Different asymmetric scenarii inclusive of the Voronoi region exploited in this report ($d_1 \neq d_2$).

meet the lighting requirement by allocating suitable values to $\varepsilon_j$, then the attenuation that $|\mathbf{z}_j|$ has suffered from will then be corrected by $\varepsilon_j$ to keep $\mathbf{x} = \varepsilon_j|\mathbf{z}_j|$ constant $\forall j$.

## III. Background of error probability and Euclidean distance

The performance of a communication system is related to the distance from the transmitted symbol to the decision boundaries. Hence, the performance of both PSK and CSK is related to the minimum distance between nearest points in the constellation. We quickly revisit the error probability theory and look into the computation technique suitable for non-symmetric constellations. The reason being that the *M*PSK-CSK constellation obtained might not be symmetric. We re-introduce the notions of Voronoi region and error probability. The voronoi region, $v$ defines the region of the constellation within which the transmitted symbol is correctly detected. The transmission system faces errors if the noise vector moves the symbol $\mathbf{s}_j$ outside of $v$. In Fig. 3, the three hatched areas represent Voronoi regions for one and two boundaries, in asymmetric scenarii in the transmitter constellation. In the following cases, we show the principle used in the computation of the probability of error proposed in this paper, to evaluate the design.

### A. Case 1: One boundary

Fig. 3-($i$) shows a constellation having one boundary. The noise $n_2$ does not affect the transmission of $\mathbf{s}_j$. The probability of error is defined by

$$\begin{aligned} p_e &= p_r\{n_1 > d\}, \\ &= Q\Big(\frac{d}{\sigma}\Big), \\ &= Q\Big(\frac{d}{\sqrt{N_0}}\Big). \end{aligned} \tag{1}$$

where Q($\alpha$) is the tail probability of the standard normal distribution given by

$$Q(\alpha) = \frac{1}{\sqrt{2\pi}} \int_{\alpha}^{\infty} e^{-\frac{\alpha^2}{2}} d\alpha. \tag{2}$$

### B. Case 2: Two parallel boundaries

A constellation having two parallel boundaries is shown in Fig. 3-($ii$). As in *case 1*, $n_2$ does not affect the transmission of $\mathbf{s}_j$. The probability of error is defined by

$$\begin{aligned} p_e &= p_r\{n_1 < -d_2 \text{ or } n_1 > d_1\}, \\ &= Q\Big(\frac{d_1}{\sqrt{N_0}}\Big) + Q\Big(\frac{d_2}{\sqrt{N_0}}\Big). \end{aligned} \tag{3}$$

### C. Case 3: Two perpendicular boundaries

A constellation including two perpendicular boundaries is shown in Fig. 3-($iii$). Unlike the first two cases, $n_2$ plays a role in the transmission of $\mathbf{s}_j$. In this case, we compute the error by doing $p_e = 1 - p_{[C]}$ where $p_{[C]}$ is the probability of correct decision.

$$\begin{aligned} p_{[C]} &= p_r\{n_1 < -d_2 \text{ and } n_1 < d_1\}, \\ &= p_r[n_1 < -d_2] \times p_r[n_1 < d_1], \\ &= \Big(1 - Q\Big(\frac{d_1}{\sqrt{N_0}}\Big)\Big)\Big(1 - Q\Big(\frac{d_2}{\sqrt{N_0}}\Big)\Big), \end{aligned} \tag{4}$$

then, we get

$$\begin{aligned} p_e &= 1 - \Big(1 - Q\Big(\frac{d_1}{\sqrt{N_0}}\Big)\Big)\Big(1 - Q\Big(\frac{d_2}{\sqrt{N_0}}\Big)\Big), \\ &= Q\Big(\frac{d_1}{\sqrt{N_0}}\Big)\Big) + Q\Big(\frac{d_2}{\sqrt{N_0}}\Big) - Q\Big(\frac{d_1}{\sqrt{N_0}}\Big)\Big)Q\Big(\frac{d_2}{\sqrt{N_0}}\Big). \end{aligned} \tag{5}$$

## IV. *M*PSK-CSK constellation design

### A. Constellation design

After the conversion of PSK symbols to colors (HSV) and from HSV to RGB, the colors form an ellipse in the RGB plan. The constellation is very similar to that of a PSK constellation. The similarities are found in the distance from the center of the circle to the points. That distance should be the same for any point. Fig. 4 shows four constellations corresponding to the *B*PSK-CSK in Fig. 4-a), *Q*PSK-CSK in Fig. 4-b), *8*PSK-CSK in Fig. 4-c) and *16*PSK-CSK in Fig. 4-d). Fig. 4-a) and 4-b) correspond to the "*One boundary*" and "*Two perpendicular boundaries*" cases analytically presented by (1) and (5), respectively. (5) also corresponds better to the case of *8*PSK-CSK shown in Fig. 4-c) and (3) if used to approximately analyze the constellation shown in Fig. 4-d).

### B. Euclidean distance optimization

*1) Performances analysis:*
The half-cone shown in Fig. 2 permits us to map PSK symbols to colors in the HSV colors space. It is done in such a way that the argument of the complex number corresponds to the hue of the HSV and the other parameters are defined by $V(\mathbf{x}) = 0.5 + 0.5\cos[2\pi(\ln(1 + |\mathbf{x}|))]$ and $S(\mathbf{x}) = 0.5 + 0.5\sin[2\pi(\ln(1 + |\mathbf{x}|))]$, where $\mathbf{x} = \varepsilon_j|\mathbf{z}_j|$. The

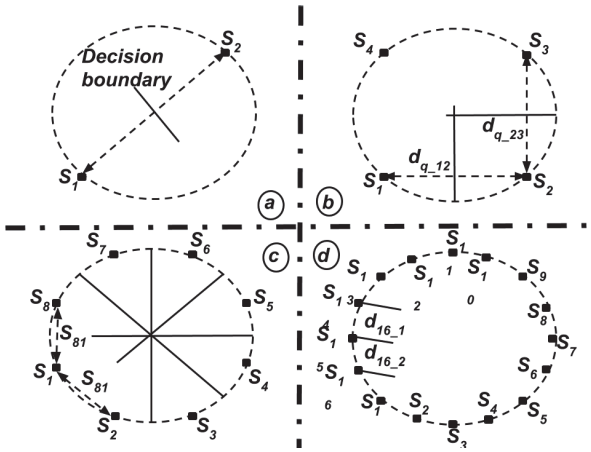


Figure 4. Constellations for: a) *B*PSK-CSK, b) *Q*PSK-CSK, c) *8*PSK-CSK, and d) *16*PSK-CSK.

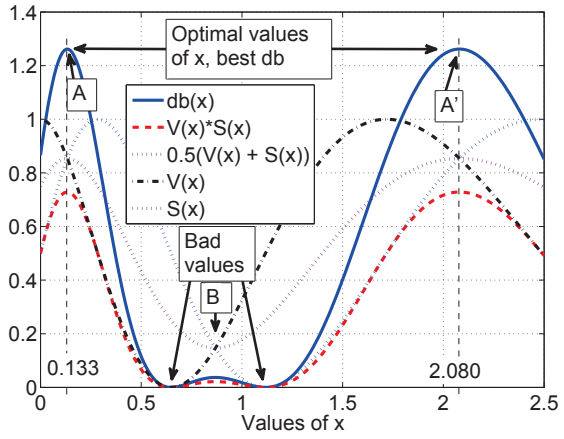


Figure 5. Variation of the distance $d_b$ between two nearest points in a two-point PSK-CSK constellation. $V(\mathbf{x})$, $S(\mathbf{x})$, $V(\mathbf{x})S(\mathbf{x})$ and $0.5(V(\mathbf{x})+S(\mathbf{x}))$ are also presented. Figure adapted and improved from [23].

Euclidean distance between symbols in *B*PSK-CSK computed in the RGB color space is given by [23]

$$d_b(\mathbf{x}) = \sqrt{2}(0.25)\big|V(\mathbf{x})S(\mathbf{x})\big|. \tag{6}$$

$d_b(\mathbf{x})$ is derived from the algorithm used to convert PSK complex symbols to colors [11], [12] and the one use in HSV to RGB conversion. We apply the conversion algorithm to the two symbols detected over the PLC channel (*B*PSK-CSK) and then compute the distance $d_b$ in the RGB plan, which varies with $\mathbf{z}_j$. The two symbols have the same value $V$ and the same saturation $S$ since they are situated on the same plate and on the same circle. In any *M*PSK-CSK optimal design, the Euclidean distance $d_b$ computed in the *B*PSK-CSK constellation will determine the performance of the system. We then analyze $V(\mathbf{x})$ and $S(\mathbf{x})$ with the aim of maximizing $d_b$. It suffices to maximize the product $V(\mathbf{x}) \times S(\mathbf{x})$. The maximum value of $d_b$ will also correspond to the maximum average of $V(\mathbf{x})$ and $S(\mathbf{x})$ given by $0.5[V(\mathbf{x}) + S(\mathbf{x})]$. Fortunately, this will be the best trade-off between illumination and communication. We solve the optimization problem and

Table I
SEVEN FIRST OPTIMAL VALUES OF $x$ PROVIDING $d_b$ = 1.2619

| $n$ | 1 | 2 | 3 | 4 | 5 | 6 | 7 |
|---|---|---|---|---|---|---|---|
| $\mathbf{x}$ | 0.133 | 2.080 | 7.372 | 21.759 | 60.867 | 167.16 | 456.14 |

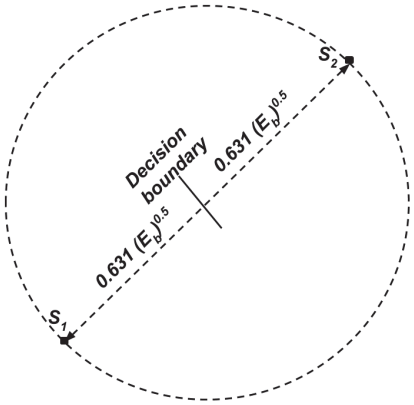


Figure 6. Constellation of *B*PSK-CSK with optimized distance (expansion of Fig. 4-a)

represent $V(\mathbf{x})$, $S(\mathbf{x})$, $V(\mathbf{x})S(\mathbf{x})$, $0.5(V(\mathbf{x})+S(\mathbf{x}))$ and $d_b(\mathbf{x})$ in Fig. 5. As mentioned above, the optimal $d_b$ is found by maximizing $V(\mathbf{x})S(\mathbf{x})$ or equaling ($V(\mathbf{x})$ and $S(\mathbf{x})$). By equaling $V(\mathbf{x})$ and $S(\mathbf{x})$, we solve $\cos[2\pi(\ln(1+|\mathbf{x}|))] = \sin[2\pi(\ln(1+|\mathbf{x}|))]$ and the general solution giving all crossing points (A, B and A$'$ in Fig. 5) of $V(\mathbf{x})$ and $S(\mathbf{x})$ is given by

$$\mathbf{x} = e^{\frac{n}{2}-\frac{7}{8}} - 1 \ (\text{n}\in \mathbb{Z}). \tag{7}$$

However, we are interested in the values of $x$ that maximize $0.5[(V(\mathbf{x}) + S(\mathbf{x})]$ and $V(\mathbf{x})S(\mathbf{x})$. They are given by

$$\mathbf{x} = e^{n+\frac{1}{8}} - 1 \ (\text{n}\in \mathbb{N}), \tag{8}$$

and correspond to points A and A' in Fig. 5. In Table I, we present the first seven values of $\mathbf{x}$ that maximize $0.5(V(\mathbf{x}) + S(\mathbf{x}))$ and $V(\mathbf{x})S(\mathbf{x})$. All these values provide the best $d_b$ which is 1.2619 for a normalized bit energy, and corresponds to one wave of $V(\mathbf{x})$ and $S(\mathbf{x})$, respectively. We have shown how the distance between two nearest symbols vary with $\mathbf{x} = \varepsilon|\mathbf{z}_j|$. Now we analyze the distance in 4, 8 and 16 points. For any of the values of $\mathbf{x}$ given in Table I, the distances shown in Fig. 4 are $d_{q\_12} = d_{q\_23}$ = 0.8140, $d_{8\_1}$ = 0.4070, $d_{8\_2}$ = 0.5460, $d_{16\_1}$ = 0.2035 and $d_{16\_2}$ = 0.2730. They are calculated between a point and its nearest neighbors in *B*PSK-CSK, *Q*PSK-CSK, *8*PSK-CSK and *16*PSK-CSK constellations, respectively. We can then express $d_{q\_12}$, $d_{q\_23}$, $d_{8\_1}$, $d_{8\_2}$, $d_{16\_1}$ and $d_{16\_2}$ using $d_b$ as follows [22], [23]

$$d_b \approx \begin{cases} \rho d_{q\_12} = \rho d_{q\_23}, \\ 2\rho d_{8\_1}, \\ \gamma d_{8\_2}, \\ 4\rho d_{16\_1}, \\ 2\gamma d_{16\_2}, \end{cases} \tag{9}$$

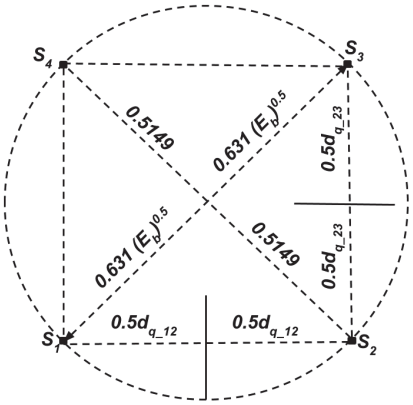


Figure 7. Constellation of *Q*PSK-CSK with optimized distances (expansion of Fig. 4-b)

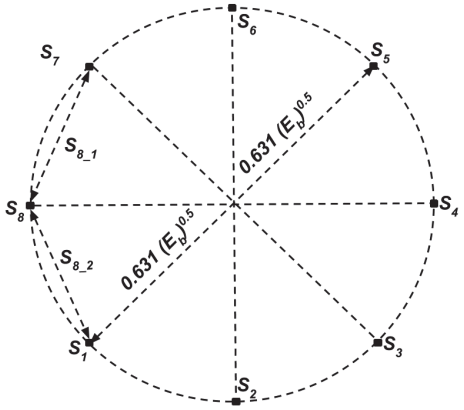


Figure 8. Constellation of *8*PSK-CSK with optimized distances (expansion of Fig. 4-c)

where $\rho \approx 1.55$ and $\gamma \approx 2.31$ and represent respectively ratios between QPSK, 8PSK and BPSK minimum distances. The noise being defined by its variance $\sigma^2$ and its power spectral density $N_0$ related by $\sigma^2 = N_0/2$, we apply (1) to Fig. 6, which is an expansion of Fig. 4-a, and get

$$p_{e\_2} = Q\Big(\frac{1.2619\sqrt{E_b}}{\sqrt{2N_0}}\Big). \tag{10}$$

We also apply (3) to Fig. 7, which is an expansion of Fig. 4-b and it leads to

$$p_{e\_4} \approx 2Q\Big(\frac{1.2619\sqrt{E_b}}{\rho\sqrt{2N_0}}\Big) + \Big[Q\Big(\frac{1.2619\sqrt{E_b}}{\rho\sqrt{2N_0}}\Big)\Big]^2, \tag{11}$$

and finally, (5) is applied to Fig. 8, expansion of Fig. 4-c and it helps to derive the bit error probability expanded as

$$\begin{aligned} p_{e\_8} \approx \frac{1}{4}\Big[2Q\Big(\frac{1.2619\sqrt{E_b}}{\gamma\sqrt{2N_0}}\Big) + \Big[Q\Big(\frac{1.2619\sqrt{E_b}}{\gamma\sqrt{2N_0}}\Big)\Big]^2\Big] \\ + \frac{1}{4}\Big[2Q\Big(\frac{1.2619\sqrt{E_b}}{2\rho\sqrt{2N_0}}\Big) + \Big[Q\Big(\frac{1.2619\sqrt{E_b}}{2\rho\sqrt{2N_0}}\Big)\Big]^2\Big] \\ + \frac{1}{2}\Big[Q\Big(\frac{1.2619\sqrt{E_b}}{2\rho\sqrt{2N_0}}\Big) + Q\Big(\frac{1.2619\sqrt{E_b}}{\gamma\sqrt{2N_0}}\Big) \\ - Q\Big(\frac{1.2619\sqrt{E_b}}{2\rho\sqrt{2N_0}}\Big)Q\Big(\frac{1.2619\sqrt{E_b}}{\gamma\sqrt{2N_0}}\Big)\Big], \end{aligned} \tag{12}$$

and

$$\begin{aligned} p_{e\_16} = \frac{3}{2}Q\Big(\frac{1.2619\sqrt{E_b}}{2\gamma\sqrt{2N_0}}\Big) + \frac{1}{2}\Big[Q\Big(\frac{1.2619\sqrt{E_b}}{4\rho\sqrt{2N_0}}\Big)\Big]^2 \\ + \frac{1}{2}\Big[Q\Big(\frac{1.2619\sqrt{E_b}}{4\rho\sqrt{2N_0}}\Big) \\ - Q\Big(\frac{1.2619\sqrt{E_b}}{4\rho\sqrt{2N_0}}\Big)Q\Big(\frac{1.2619\sqrt{E_b}}{2\gamma\sqrt{2N_0}}\Big)\Big], \end{aligned} \tag{13}$$

for *B*PSK-CSK (10), *Q*PSK-CSK (11), *8*PSK-CSK (12), and *16*PSK-CSK (13), respectively. We compare in Fig. 9, the performances of the four *M*PSK-CSK constellation size to that of the theoretical *B*PSK. The expression of $d_b$ presented in (6) explains the performance of *B*PSK-CSK compared to that of the theoretical *B*PSK. For the other constellation sizes,

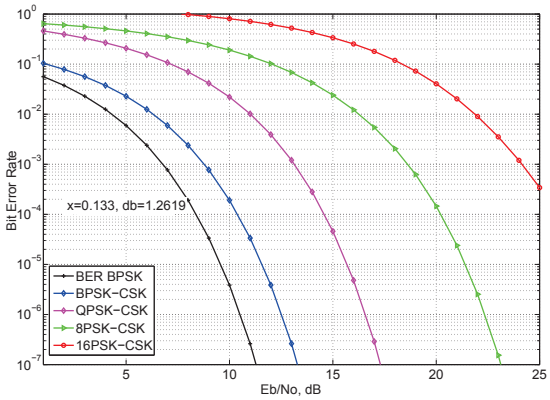


Figure 9. Comparison between *B*PSK, *B*PSK-CSK, *Q*PSK-CSK, *8*PSK-CSK and *16*PSK-CSK for **x** = 0.133.

it is obvious that constellation size increases at the expense of the performance. We empirically generalize this analysis by deducing the general probability for an *M*PSK-CSK and get two series that vary with the nature of $m$ in $M = 2^m$. The first series corresponds to even values of $m$ and the second fits in the case of odd values of $m$. We show in Figs. 10 and 11, the prediction of the performance of *M*PSK-CSK systems for $\{8, 32, 128, 512\}$ and $\{16, 64, 256, 1024\}$. For the sake of consistency over the vertical axis, we scale the horizontal axis from 15 to 40. The curves confirm better performance of the smaller sizes of the constellation when compared to bigger ones.

*2) Generalization:*

We assume perfect conversion algorithm between complex symbols to the HSV color space and perfect HSV to RGB conversion matrix. This implies that symmetric *M*PSK-CSK constellations are obtained. The general expression of the error probability can then be approximated by

$$p_e \approx 2Q\left[\sqrt{0.4\frac{E_b}{N_0}}\sin\left(\frac{\pi}{M}\right)\right]. \tag{14}$$

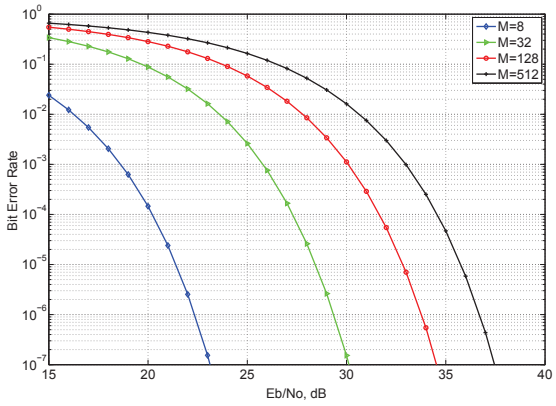


Figure 10. Performance of $M$PSK-CSK for even values of $n$ ($M$ = 8, 32, 128, 512).

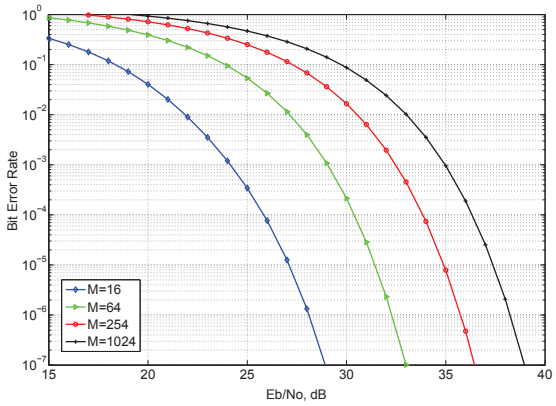


Figure 11. Performance of $M$PSK-CSK for odd values of $n$ ($M$ = 16, 64, 256, 1024).

## V. Conclusion

This paper proposes the design of constellations for $M$PSK-CSK for hybrid PLC-VLC cascaded systems. The aim is to design an efficient constellation for hybrid PLC-VLC cascaded systems. A mapping technique exploiting the HSV color space is used in PSK to CSK conversion. PSK and CSK are used over PLC and VLC channels respectively. The PSK-CSK conversion algorithm produces a distance $d_b$ that varies with the modulus of the PSK complex symbol, which is modulated by a correcting factor $\varepsilon$ to meet lighting and communication requirements. The optimization problem obtained is solved and the best distance between nearest symbols is $1.2619\sqrt{E_b}$ corresponding to $\mathbf{x} = \{0.133,\ 2.080,\ 7.372,\ 21.759,\ 60.867,\ 167.16,\ \ldots\}$. We then analyze performances of $M$PSK systems for $d_b = 1.2619\sqrt{E_b}$. For values of $M$ greater than 4, we give a general expression for odd and even values of $m$ separately, then we derive the probability in each case, and a general expression is proposed.

## References


[1] M. M. Rahman, C. S. Hong, S. Lee, J. Lee, M. A. Razzaque, and J. H. Kim, "Medium access control for power line communications: an overview of the IEEE 1901 and ITU-T G.hn standards," *IEEE Commun. Mag.*, vol. 49, no. 6, pp. 183–191, Jun. 2011.

[2] H. A. Latchman, S. Katar, L. Yonge, and S. Gavette, *IEEE 1901*. Wiley-IEEE Press, 2013. [Online]. Available: http://ieeexplore.ieee.org/xpl/articleDetails.jsp?arnumber=6645463

[3] S. Goldfisher and S. Tanabe, "IEEE 1901 Access System: An overview of its uniqueness and motivation," *IEEE Commun. Mag.*, vol. 48, no. 10, pp. 150–157, Oct. 2010.

[4] V. Oksman and S. Galli, "G.hn: The New ITU-T Home Networking Standard," *IEEE Commun. Mag.*, vol. 47, no. 10, pp. 138–145, Oct. 2009.

[5] "IEEE standard for local and metropolitan area networks–part 15.7: short-range wireless optical communication using visible light," *IEEE Std 802.15.7-2011*, pp. 1–309, Sep. 2011.

[6] R. J. Drost and B. M. Sadler, "Constellation design for channel precompensation in multi-wavelength visible light communications," *IEEE Trans. Commun.*, vol. 62, no. 6, pp. 1995–2005, Jun. 2014.

[7] R. Singh, T. O'Farrell, and J. P. R. David, "Performance evaluation of IEEE 802.15.7 CSK physical layer," in *Proc. IEEE GLOBECOM Workshops*, Atlanta, GA, USA, Dec. 9-13, 2013, pp. 1064–1069.

[8] E. Monteiro and S. Hranilovic, "Design and implementation of color-shift keying for visible light communications," *IEEE J. Lightw. Technol.*, vol. 32, no. 10, pp. 2053–2060, May 2014.

[9] S. Rajagopal, R. D. Roberts, and S. K. Lim, "IEEE 802.15.7 visible light communication: modulation schemes and dimming support," *IEEE Commun. Mag.*, vol. 50, no. 3, pp. 72–82, Mar. 2012.

[10] R. D. Roberts, S. Rajagopal, and S. K. Lim, "IEEE 802.15.7 physical layer summary," in *Proc. IEEE GLOBECOM Workshops*, Houston, TX, USA, Dec. 5-9, 2011, pp. 772–776.

[11] F. A. Farris, *Visualizing Complex-Valued Functions in the Plane*, AMC 10 1997.

[12] J. B. Conway, *Functions of One Complex Variable II*. Springer Science and Business Media, 1995, vol. 2.

[13] T. Komine and M. Nakagawa, "Integrated System of White LED Visible-Light Communication and Power-Line Communication," *IEEE Trans. Consum. Electron.*, vol. 49, no. 1, pp. 71–79, Feb. 2003.

[14] J. Song, W. Ding, F. Yang, H. Yang, B. Yu, and H. Zhang, "An Indoor Broadband Broadcasting System Based on PLC and VLC," *IEEE Trans. Broadcast.*, vol. 61, no. 2, pp. 299–308, Jun. 2015.

[15] W. Ding, F. Yang, H. Yang, J. Wang, X. Wang, X. Zhang, and J. Song, "A hybrid power line and visible light communication system for indoor hospital applications," *Comput. in Industry*, vol. 68, pp. 170–178, 2015.

[16] A. R. Ndjiongue, T. Shongwe, H. C. Ferreira, T. M. N. Ngatched, and A. J. H. Vinck, "Cascaded PLC-VLC Channel Using OFDM and CSK Techniques," in *Proc. IEEE GLOBECOM Conf.*, San Diego, CA, USA, Dec. 6-10, 2015, pp. 1–6.

[17] H. Ma, L. Lampe, and S. Hranilovic, "Integration of Indoor Visible Light and Power Line Communication Systems," in *Proc. 17th IEEE ISPLC Conf.*, Johannesburg, South Africa, Mar. 24-27, 2013, pp. 291–296.

[18] M. S. A. Mossaad, S. Hranilovic, and L. Lampe, "Amplify-and-Forward Integration of Power Line and Visible Light Communications," in *Proc. IEEE Global Conf. Signal and Inf. Process. (GlobalSIP)*, Orlando, FL, USA, Dec. 14-16, 2015, pp. 1322–1326.

[19] A. R. Ndjiongue, H. C. Ferreira, K. Ouahada, and A. J. H. Vinckz, "FLow-Complexity SOCPBFSK-OOK Interface Between PLC and VLC Channels for Low Data Rate Transmission Applications," in *Proc. 18th IEEE ISPLC Conf.*, Glasgow, Scotland, UK, Mar. 30-Apr. 2, 2014, pp. 226–231.

[20] A. D. Familua, A. R. Ndjiongue, K. Ogunyanda, L. Cheng, H. C. Ferreira, and T. G. Swart, "A Semi-Hidden Markov Modeling of a Low Complexity FSK-OOK in-House PLC and VLC Integration," in *Proc. 19th IEEE ISPLC Conf.*, Austin, TX, USA, Mar. 29-31, 2015, pp. 199–204.

[21] A. R. Ndjiongue, H. C. Ferreira, and T. Shongwe, "Inter-Building PLC-VLC Integration Based on PSK and CSK Techniques," in *Proc. 20th IEEE ISPLC Conf.*, Bottrop, Germany, Mar. 20-23, 2016, pp. 31–36.

[22] A. R. Ndjiongue, H. C. Ferreira, T. Shongwe, T. Ngatched, and A. J. Han Vinck, "PSK to CSK Mapping for Hybrid Systems Involving the Radio Frequency and the Visible Spectrum," *Telecommun. Syst.*, May 2016, Online First.

[23] A. R. Ndjiongue, T. Shongwe, and H. C. Ferreira, "Closed-Form BER expressions for HSV based MPSK-CSK Systems," *IEEE Commun. Lett.*, vol. PP, no. 99, pp. 1–1, 2017.

# Constellation Design for Cascaded *M*PSK-CSK Systems

A. R. Ndjiongue*, H. C. Ferreira* and Telex M. N. Ngatched⊛
* Department of Electrical and Electronic Engineering Science, University of Johannesburg,
P.O. Box 524, Auckland Park, 2006, Johannesburg, South Africa.
⊛ Faculty of Engineering and Applied Science, Memorial University,
St. John's, NL A1B 3X5, Canada.
Emails: {arrichard,hcferreira}@uj.ac.za,tngatched@grenfell.mun.ca

***Abstract*—This paper proposes a constellation design for color shift keying (CSK) based on phase shift keying (PSK) conversion, to be used in cascaded power line communications (PLC) and visible light communications (VLC) systems integration. We optimize the design of *M*PSK-CSK constellations and analyze the performance of *M*PSK-CSK systems based on the optimized Euclidean distance calculated on the red-green-blue (RGB) color space.**

***Index Terms*—*M*PSK-CSK constellation design, hybrid PLC-VLC systems, *M*PSK-CSK systems, cascaded channels, PLC-VLC interface. PSK and CSK schemes, RGB colors space.**

## I. Introduction

Visible light communications (VLC) and power line communications (PLC) present many similarities including that they are parts of the electrical power system and that they both represent a communication technology. Interfacing both technologies has become one of the major research fields in telecommunication engineering, owing firstly to the advantages provided by both technologies when taken individually (for example, ubiquitous power line infrastructure and power saving light emitting diodes (LEDs)), secondly to the physical link between the power wires and the light source. Added to these reasons, PLC technology could be used as return path in VLC duplex transmissions or VLC could be used to connect the PLC end user. Additionally, PLC technology is seen as the best backbone for VLC technology.

From the PLC standards point of view, IEEE 1901 [1]–[3], ITU-T G.9955/56, ITU-T G.9960/61 [4], G3-PLC, PRIME and HOMEPLUG, propose modulation techniques including orthogonal frequency division multiplexing (OFDM) with phase shift keying (PSK), quadrature amplitude modulation (QAM) or amplitude PSK (APSK) over sub-carriers. PSK is a digital modulation technique that convey information by changing the phase of the carrier signal. PSK is very solicited in transmission systems where the amplitude of the received signal cannot be trusted, even though it is weak against phase noise. Then, PSK provides the important advantage that the amplitude of the transmitted signal does not play a major role in symbol transmission. Even though PSK is weak against phase noise, this aspect is a vital key for the report proposed in this paper.

In VLC technology, the fast increasing number of research reports shows the interest of the research community in seeing a massive deployment of the technology. Color shift keying (CSK), proposed in IEEE 802.15.7 [5] and analyzed in [6]–[10], is a digital modulation technique exploiting color variation for data transmission. The information is concealed in a color produced using red-green-blue (RGB) LEDs. The constellation in CSK fits in a triangle that is compartmented to form decision regions. CSK could be the main modulation technique to be adapted in applications such as light fidelity (Li-Fi). This scheme presents numerous advantages when compared to other modulation techniques. For example, there is no inrush current and no flickering in CSK.

In color technology, many color spaces are available to be used. They are dedicated to specific applications. For example, the Cyan-Magenta-Yellow-Key (CMYK) color model is used in printing owing to its ease to directly producing the black color. In the same sense, the hue-saturation-value (HSV) is mostly used in image detection owing to its facility to extract color parameters (*i.e* saturation, chroma, value, hue) of an image. On the other side, the RGB color space is for example exploited in color television for its ease to produce the rest of colors by modulating the intensities of the currents flowing in the circuits. The CSK technique is based on producing colors by modulating the intensities of the currents flowing in the RGB-LEDs used. Conversion matrices are available to change color space, also, algorithms are available to convert the complex plane to a color space [11], [12]. The most used conversion algorithm between complex vectors and colors is based on the color wheel and uses the HSV color space [11], [12].

A great number of research reports focusing on interfacing PLC and VLC have been proposed, [13]–[21] to mention only few of them. They all propose solutions to make possible the integration of PLC and VLC technologies. We briefly present some of the work that has been done to add value in PLC-VLC integration. [13] is one of the precursors of PLC-VLC integration. It proposes a system exploiting PSK over the PLC channel and retransmitting over the VLC channel using white LEDs, without demodulating the signal from the power-line.

978-1-5090-1525-2/17/$31.00 ©2017 IEEE

[14] proposes a novel and cost-effective indoor broadband broadcasting PLC-VLC integration while [15] focuses on applying hybrid broadband PLC-VLC systems based on OFDM modulation in hospital applications. In [16], the performance of cascaded PLC-VLC systems using OFDM and CSK is proposed. [17] reviews the state of both broadband PLC and VLC systems and proposes new directions for PLC-VLC integration. [18] applies a spatial-optical OFDM in PLC-VLC systems while [19] and [20] focus on practically implementing hybrid PLC-VLC systems based on spread frequency shift keying (SFSK) and on-off keying (OOK). In [21]–[23], a technique to map PSK symbols to colors using the color wheel and the HSV color space is proposed. It exploits the aforementioned knowledge of PSK modulation technique on the magnitude of the PSK symbol, to control transmission and lighting performances of hybrid PLC-VLC systems. In this technique, the amplitude of the *M*PSK (PLC) received symbol is altered to control both transmission and illumination over the VLC channel. Note that the technique proposed in [21]–[23], for which the constellation design is given here presents two important advantages which are: (*i*) Natural mapping between PSK and CSK implying very less processing between PLC and VLC channels (cascaded channels) and (*ii*) constant lighting provided by RGB-LEDs without using any other compensation circuit.

In this paper, we propose an optimal constellation design for such hybrid PLC-VLC systems. It is shown that the increment of *M*PSK-CSK constellation size is done at the expense of the communication performance. However, for all constellation sizes, a trade-off between communication and lighting is obtained by maximizing the product $V \times S$ of the value by the saturation or their average $0.5(V + S)$. We optimize the design of a *B*PSK-CSK constellation and apply the result to any *M*PSK-CSK constellation size. Note that the color rendering requirement and the VLC channel effect are not taken into account in this paper.

The remainder of the paper proposes a model of *M*PSK-CSK systems in Section II and gives a quick view of the background of the error probability computation in Section III. The optimized constellation design is proposed in Section IV. The Euclidean distance is analyzed and some results on analytical bit error rate (BER) are proposed. Finally, the paper is concluded in Section V.

## II. *M*PSK-CSK System Model

A model of *M*PSK-CSK interface is proposed in Fig. 1. The $j^{th}$ symbol $\mathbf{z}_j$ ($j = 0, 1, 2, \ldots, M-1$), detected over the PLC channel, essentially has a magnitude $|\mathbf{z}_j|$ and a phase $\theta_J$. The PSK demodulator does not pay attention to the value of $|\mathbf{z}_j|$. Later, we will use $|\mathbf{z}_j|$ to control lighting and transmission over the VLC channel. The algorithm used in the color wheel is based on the three following equations: $H_j = \arg(\mathbf{z}_j)$, $V_j = 0.5 + 0.5\cos(2\pi r_j)$ and $S_j = 0.5 + 0.5\sin(2\pi r_j)$. To do the mapping, the color wheel exploits the advantage that $\theta_j$ and $H_j$ are angles and vary between 0 and $\pi$. $V_j$ and $S_j$ are computed base on $r_j = 1 + \ln(1 + |\mathbf{z}_j|)$. Hence,

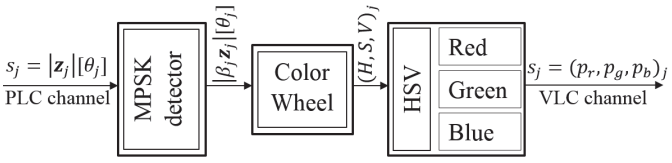


Figure 1. *M*PSK-CSK interface model showing only the blocks between PLC and VLC channels.

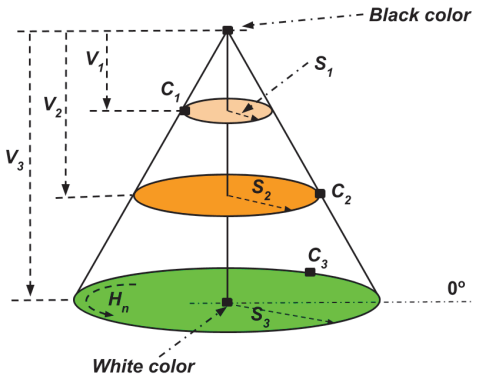


Figure 2. HSV color space represented by its half-cone.

they vary with $|\mathbf{z}_j|$. We then impose a factor $\varepsilon_j$ to modulate $V_j$ and $S_j$. $\varepsilon_j$ is an amplification factor used to repair all distortions that happened to $|\mathbf{z}_j|$ over the PLC channel, due to attenuation and noise. In the design optimization proposed in Section IV, we will show the variation of $V(\mathbf{x})$ and $S(\mathbf{x})$. We match the obtained ($H_j$,$S_j$,$V_j$) to an RGB color so that the transmission uses RGB-LEDs. Three currents are allocated to the RGB-LEDs to produce the color $\mathbf{c}_j$ corresponding to the complex symbol $\mathbf{z}_j$. Thus, the constellation of size $M$ obtained is called *M*PSK-CSK constellation. It shares its size with the original PSK constellation and with the final CSK constellation. The transmission over the VLC channel must meet the lighting requirement $[(p_r + p_g + p_b)_j = 1]$ and the communication objectives (*i.e* maximizing the minimum Euclidean distance between the nearest colors in the sender constellation). The lighting requirement is permanently met and represents one specific advantage of the HSV color space: All colors situated at the same distance from the black color are produced with the same lighting intensity (value $V$ of HSV, see Fig. 2). Fig. 2 shows the HSV half-cone. Three values of the intensity ($V_1, V_2, V_3$) and saturation ($S_1, S_2, S_3$), and the rotation direction of $H$ are shown. The axis is $White-Black$, and gives the lighting level (values of $V$) and the radii of the plates correspond to saturation levels (values of $S$). We use $\varepsilon_j$ to voluntarily vary $V_j$ and $S_j$ when needed. $\varepsilon_j$ helps keeping the product $\varepsilon_j|\mathbf{z}_j|$ constant for all PSK symbols detected over the PLC channel. Then, the main aim of the constellation design proposed in this paper is to find the best trade-off between lighting and communication. We will then

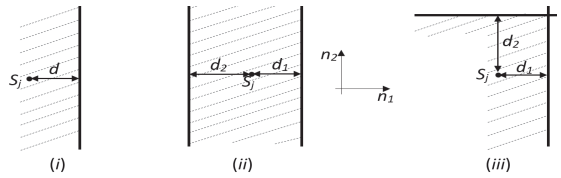


Figure 3. Different asymmetric scenarii inclusive of the Voronoi region exploited in this report ($d_1 \neq d_2$).

meet the lighting requirement by allocating suitable values to $\varepsilon_j$, then the attenuation that $|\mathbf{z}_j|$ has suffered from will then be corrected by $\varepsilon_j$ to keep $\mathbf{x} = \varepsilon_j|\mathbf{z}_j|$ constant $\forall j$.

## III. Background of error probability and Euclidean distance

The performance of a communication system is related to the distance from the transmitted symbol to the decision boundaries. Hence, the performance of both PSK and CSK is related to the minimum distance between nearest points in the constellation. We quickly revisit the error probability theory and look into the computation technique suitable for non-symmetric constellations. The reason being that the *M*PSK-CSK constellation obtained might not be symmetric. We re-introduce the notions of Voronoi region and error probability. The voronoi region, $v$ defines the region of the constellation within which the transmitted symbol is correctly detected. The transmission system faces errors if the noise vector moves the symbol $\mathbf{s}_j$ outside of $v$. In Fig. 3, the three hatched areas represent Voronoi regions for one and two boundaries, in asymmetric scenarii in the transmitter constellation. In the following cases, we show the principle used in the computation of the probability of error proposed in this paper, to evaluate the design.

### A. Case 1: One boundary

Fig. 3-($i$) shows a constellation having one boundary. The noise $n_2$ does not affect the transmission of $\mathbf{s}_j$. The probability of error is defined by

$$\begin{aligned} p_e &= p_r\{n_1 > d\}, \\ &= Q\Big(\frac{d}{\sigma}\Big), \\ &= Q\Big(\frac{d}{\sqrt{N_0}}\Big). \end{aligned} \tag{1}$$

where Q($\alpha$) is the tail probability of the standard normal distribution given by

$$Q(\alpha) = \frac{1}{\sqrt{2\pi}} \int_{\alpha}^{\infty} e^{-\frac{\alpha^2}{2}} d\alpha. \tag{2}$$

### B. Case 2: Two parallel boundaries

A constellation having two parallel boundaries is shown in Fig. 3-($ii$). As in *case 1*, $n_2$ does not affect the transmission of $\mathbf{s}_j$. The probability of error is defined by

$$\begin{aligned} p_e &= p_r\{n_1 < -d_2 \text{ or } n_1 > d_1\}, \\ &= Q\Big(\frac{d_1}{\sqrt{N_0}}\Big) + Q\Big(\frac{d_2}{\sqrt{N_0}}\Big). \end{aligned} \tag{3}$$

### C. Case 3: Two perpendicular boundaries

A constellation including two perpendicular boundaries is shown in Fig. 3-($iii$). Unlike the first two cases, $n_2$ plays a role in the transmission of $\mathbf{s}_j$. In this case, we compute the error by doing $p_e = 1 - p_{[C]}$ where $p_{[C]}$ is the probability of correct decision.

$$\begin{aligned} p_{[C]} &= p_r\{n_1 < -d_2 \text{ and } n_1 < d_1\}, \\ &= p_r[n_1 < -d_2] \times p_r[n_1 < d_1], \\ &= \Big(1 - Q\Big(\frac{d_1}{\sqrt{N_0}}\Big)\Big)\Big(1 - Q\Big(\frac{d_2}{\sqrt{N_0}}\Big)\Big), \end{aligned} \tag{4}$$

then, we get

$$\begin{aligned} p_e &= 1 - \Big(1 - Q\Big(\frac{d_1}{\sqrt{N_0}}\Big)\Big)\Big(1 - Q\Big(\frac{d_2}{\sqrt{N_0}}\Big)\Big), \\ &= Q\Big(\frac{d_1}{\sqrt{N_0}}\Big)\Big) + Q\Big(\frac{d_2}{\sqrt{N_0}}\Big) - Q\Big(\frac{d_1}{\sqrt{N_0}}\Big)\Big)Q\Big(\frac{d_2}{\sqrt{N_0}}\Big). \end{aligned} \tag{5}$$

## IV. *M*PSK-CSK constellation design

### A. Constellation design

After the conversion of PSK symbols to colors (HSV) and from HSV to RGB, the colors form an ellipse in the RGB plan. The constellation is very similar to that of a PSK constellation. The similarities are found in the distance from the center of the circle to the points. That distance should be the same for any point. Fig. 4 shows four constellations corresponding to the *B*PSK-CSK in Fig. 4-a), *Q*PSK-CSK in Fig. 4-b), *8*PSK-CSK in Fig. 4-c) and *16*PSK-CSK in Fig. 4-d). Fig. 4-a) and 4-b) correspond to the "*One boundary*" and "*Two perpendicular boundaries*" cases analytically presented by (1) and (5), respectively. (5) also corresponds better to the case of *8*PSK-CSK shown in Fig. 4-c) and (3) if used to approximately analyze the constellation shown in Fig. 4-d).

### B. Euclidean distance optimization

*1) Performances analysis:*

The half-cone shown in Fig. 2 permits us to map PSK symbols to colors in the HSV colors space. It is done in such a way that the argument of the complex number corresponds to the hue of the HSV and the other parameters are defined by $V(\mathbf{x}) = 0.5 + 0.5\cos[2\pi(\ln(1 + |\mathbf{x}|))]$ and $S(\mathbf{x}) = 0.5 + 0.5\sin[2\pi(\ln(1 + |\mathbf{x}|))]$, where $\mathbf{x} = \varepsilon_j|\mathbf{z}_j|$. The

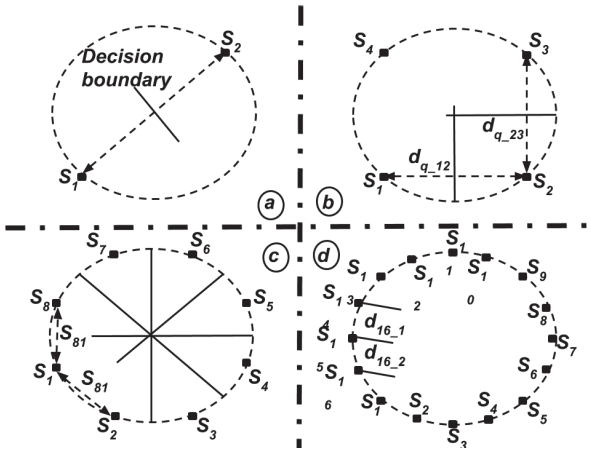


Figure 4. Constellations for: a) *B*PSK-CSK, b) *Q*PSK-CSK, c) *8*PSK-CSK, and d) *16*PSK-CSK.

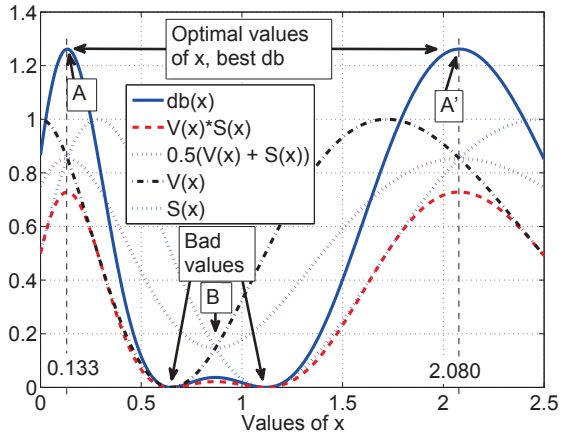


Figure 5. Variation of the distance $d_b$ between two nearest points in a two-point PSK-CSK constellation. $V(\mathbf{x})$, $S(\mathbf{x})$, $V(\mathbf{x})S(\mathbf{x})$ and $0.5(V(\mathbf{x})+S(\mathbf{x}))$ are also presented. Figure adapted and improved from [23].

Euclidean distance between symbols in *B*PSK-CSK computed in the RGB color space is given by [23]

$$d_b(\mathbf{x}) = \sqrt{2}(0.25)\big|V(\mathbf{x})S(\mathbf{x})\big|. \tag{6}$$

$d_b(\mathbf{x})$ is derived from the algorithm used to convert PSK complex symbols to colors [11], [12] and the one use in HSV to RGB conversion. We apply the conversion algorithm to the two symbols detected over the PLC channel (*B*PSK-CSK) and then compute the distance $d_b$ in the RGB plan, which varies with $\mathbf{z}_j$. The two symbols have the same value $V$ and the same saturation $S$ since they are situated on the same plate and on the same circle. In any *M*PSK-CSK optimal design, the Euclidean distance $d_b$ computed in the *B*PSK-CSK constellation will determine the performance of the system. We then analyze $V(\mathbf{x})$ and $S(\mathbf{x})$ with the aim of maximizing $d_b$. It suffices to maximize the product $V(\mathbf{x}) \times S(\mathbf{x})$. The maximum value of $d_b$ will also correspond to the maximum average of $V(\mathbf{x})$ and $S(\mathbf{x})$ given by $0.5[V(\mathbf{x}) + S(\mathbf{x})]$. Fortunately, this will be the best trade-off between illumination and communication. We solve the optimization problem and

Table I
SEVEN FIRST OPTIMAL VALUES OF $x$ PROVIDING $d_b$ = 1.2619

| $n$ | 1 | 2 | 3 | 4 | 5 | 6 | 7 |
|---|---|---|---|---|---|---|---|
| $\mathbf{x}$ | 0.133 | 2.080 | 7.372 | 21.759 | 60.867 | 167.16 | 456.14 |

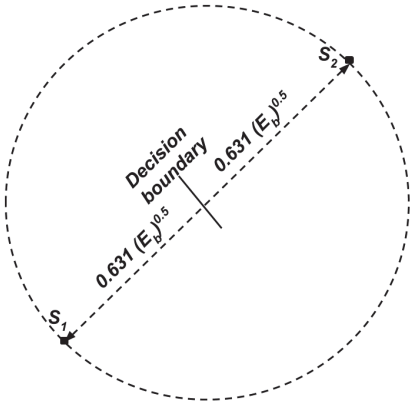


Figure 6. Constellation of *B*PSK-CSK with optimized distance (expansion of Fig. 4-a)

represent $V(\mathbf{x})$, $S(\mathbf{x})$, $V(\mathbf{x})S(\mathbf{x})$, $0.5(V(\mathbf{x})+S(\mathbf{x}))$ and $d_b(\mathbf{x})$ in Fig. 5. As mentioned above, the optimal $d_b$ is found by maximizing $V(\mathbf{x})S(\mathbf{x})$ or equaling ($V(\mathbf{x})$ and $S(\mathbf{x})$). By equaling $V(\mathbf{x})$ and $S(\mathbf{x})$, we solve $\cos[2\pi(\ln(1+|\mathbf{x}|))] = \sin[2\pi(\ln(1+|\mathbf{x}|))]$ and the general solution giving all crossing points (A, B and A$'$ in Fig. 5) of $V(\mathbf{x})$ and $S(\mathbf{x})$ is given by

$$\mathbf{x} = e^{\frac{n}{2}-\frac{7}{8}} - 1 \ (\text{n}\in \mathbb{Z}). \tag{7}$$

However, we are interested in the values of $x$ that maximize $0.5[(V(\mathbf{x}) + S(\mathbf{x})]$ and $V(\mathbf{x})S(\mathbf{x})$. They are given by

$$\mathbf{x} = e^{n+\frac{1}{8}} - 1 \ (\text{n}\in \mathbb{N}), \tag{8}$$

and correspond to points A and A' in Fig. 5. In Table I, we present the first seven values of $\mathbf{x}$ that maximize $0.5(V(\mathbf{x}) + S(\mathbf{x}))$ and $V(\mathbf{x})S(\mathbf{x})$. All these values provide the best $d_b$ which is 1.2619 for a normalized bit energy, and corresponds to one wave of $V(\mathbf{x})$ and $S(\mathbf{x})$, respectively. We have shown how the distance between two nearest symbols vary with $\mathbf{x} = \varepsilon|\mathbf{z}_j|$. Now we analyze the distance in 4, 8 and 16 points. For any of the values of $\mathbf{x}$ given in Table I, the distances shown in Fig. 4 are $d_{q\_12} = d_{q\_23}$ = 0.8140, $d_{8\_1}$ = 0.4070, $d_{8\_2}$ = 0.5460, $d_{16\_1}$ = 0.2035 and $d_{16\_2}$ = 0.2730. They are calculated between a point and its nearest neighbors in *B*PSK-CSK, *Q*PSK-CSK, *8*PSK-CSK and *16*PSK-CSK constellations, respectively. We can then express $d_{q\_12}$, $d_{q\_23}$, $d_{8\_1}$, $d_{8\_2}$, $d_{16\_1}$ and $d_{16\_2}$ using $d_b$ as follows [22], [23]

$$d_b \approx \begin{cases} \rho d_{q\_12} = \rho d_{q\_23}, \\ 2\rho d_{8\_1}, \\ \gamma d_{8\_2}, \\ 4\rho d_{16\_1}, \\ 2\gamma d_{16\_2}, \end{cases} \tag{9}$$

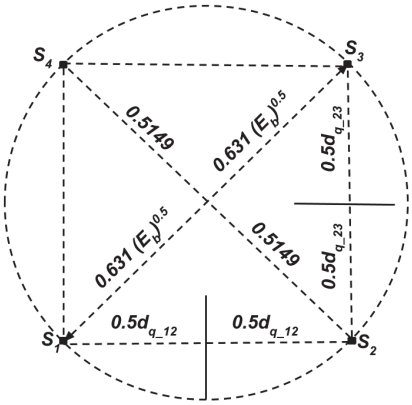


Figure 7. Constellation of *Q*PSK-CSK with optimized distances (expansion of Fig. 4-b)

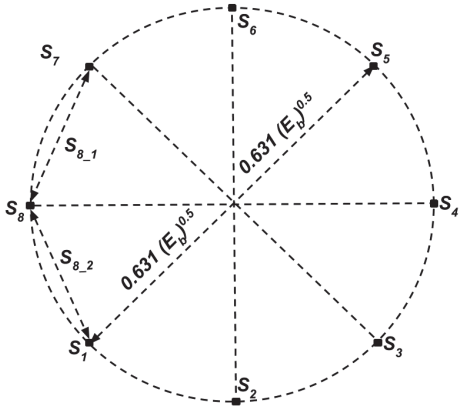


Figure 8. Constellation of *8*PSK-CSK with optimized distances (expansion of Fig. 4-c)

where $\rho \approx 1.55$ and $\gamma \approx 2.31$ and represent respectively ratios between QPSK, 8PSK and BPSK minimum distances. The noise being defined by its variance $\sigma^2$ and its power spectral density $N_0$ related by $\sigma^2 = N_0/2$, we apply (1) to Fig. 6, which is an expansion of Fig. 4-a, and get

$$p_{e\_2} = Q\Big(\frac{1.2619\sqrt{E_b}}{\sqrt{2N_0}}\Big). \tag{10}$$

We also apply (3) to Fig. 7, which is an expansion of Fig. 4-b and it leads to

$$p_{e\_4} \approx 2Q\Big(\frac{1.2619\sqrt{E_b}}{\rho\sqrt{2N_0}}\Big) + \Big[Q\Big(\frac{1.2619\sqrt{E_b}}{\rho\sqrt{2N_0}}\Big)\Big]^2, \tag{11}$$

and finally, (5) is applied to Fig. 8, expansion of Fig. 4-c and it helps to derive the bit error probability expanded as

$$\begin{aligned} p_{e\_8} \approx \frac{1}{4}\Big[&2Q\Big(\frac{1.2619\sqrt{E_b}}{\gamma\sqrt{2N_0}}\Big) + \Big[Q\Big(\frac{1.2619\sqrt{E_b}}{\gamma\sqrt{2N_0}}\Big)\Big]^2\Big] \\ &+ \frac{1}{4}\Big[2Q\Big(\frac{1.2619\sqrt{E_b}}{2\rho\sqrt{2N_0}}\Big) + \Big[Q\Big(\frac{1.2619\sqrt{E_b}}{2\rho\sqrt{2N_0}}\Big)\Big]^2\Big] \\ &+ \frac{1}{2}\Big[Q\Big(\frac{1.2619\sqrt{E_b}}{2\rho\sqrt{2N_0}}\Big) + Q\Big(\frac{1.2619\sqrt{E_b}}{\gamma\sqrt{2N_0}}\Big) \\ &- Q\Big(\frac{1.2619\sqrt{E_b}}{2\rho\sqrt{2N_0}}\Big)Q\Big(\frac{1.2619\sqrt{E_b}}{\gamma\sqrt{2N_0}}\Big)\Big], \end{aligned} \tag{12}$$

and

$$\begin{aligned} p_{e\_16} = \frac{3}{2}&Q\Big(\frac{1.2619\sqrt{E_b}}{2\gamma\sqrt{2N_0}}\Big) + \frac{1}{2}\Big[Q\Big(\frac{1.2619\sqrt{E_b}}{4\rho\sqrt{2N_0}}\Big)\Big]^2 \\ &+ \frac{1}{2}\Big[Q\Big(\frac{1.2619\sqrt{E_b}}{4\rho\sqrt{2N_0}}\Big) \\ &- Q\Big(\frac{1.2619\sqrt{E_b}}{4\rho\sqrt{2N_0}}\Big)Q\Big(\frac{1.2619\sqrt{E_b}}{2\gamma\sqrt{2N_0}}\Big)\Big], \end{aligned} \tag{13}$$

for *B*PSK-CSK (10), *Q*PSK-CSK (11), *8*PSK-CSK (12), and *16*PSK-CSK (13), respectively. We compare in Fig. 9, the performances of the four *M*PSK-CSK constellation size to that of the theoretical *B*PSK. The expression of $d_b$ presented in (6) explains the performance of *B*PSK-CSK compared to that of the theoretical *B*PSK. For the other constellation sizes,

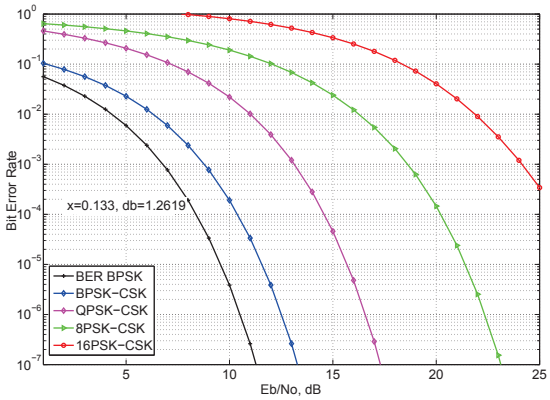


Figure 9. Comparison between *B*PSK, *B*PSK-CSK, *Q*PSK-CSK, *8*PSK-CSK and *16*PSK-CSK for **x** = 0.133.

it is obvious that constellation size increases at the expense of the performance. We empirically generalize this analysis by deducing the general probability for an *M*PSK-CSK and get two series that vary with the nature of $m$ in $M = 2^m$. The first series corresponds to even values of $m$ and the second fits in the case of odd values of $m$. We show in Figs. 10 and 11, the prediction of the performance of *M*PSK-CSK systems for $\{8, 32, 128, 512\}$ and $\{16, 64, 256, 1024\}$. For the sake of consistency over the vertical axis, we scale the horizontal axis from 15 to 40. The curves confirm better performance of the smaller sizes of the constellation when compared to bigger ones.

*2) Generalization:*

We assume perfect conversion algorithm between complex symbols to the HSV color space and perfect HSV to RGB conversion matrix. This implies that symmetric *M*PSK-CSK constellations are obtained. The general expression of the error probability can then be approximated by

$$p_e \approx 2Q\left[\sqrt{0.4\frac{E_b}{N_0}}\sin\left(\frac{\pi}{M}\right)\right]. \tag{14}$$

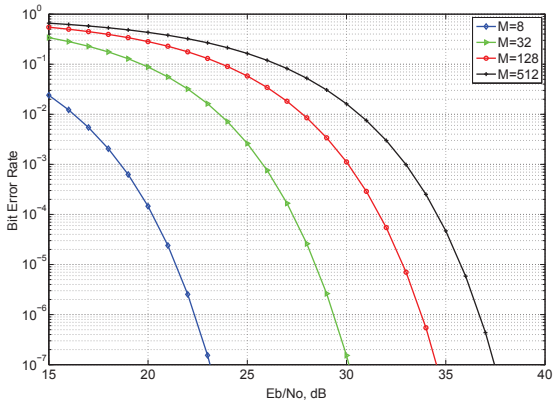


Figure 10. Performance of $M$PSK-CSK for even values of $n$ ($M$ = 8, 32, 128, 512).

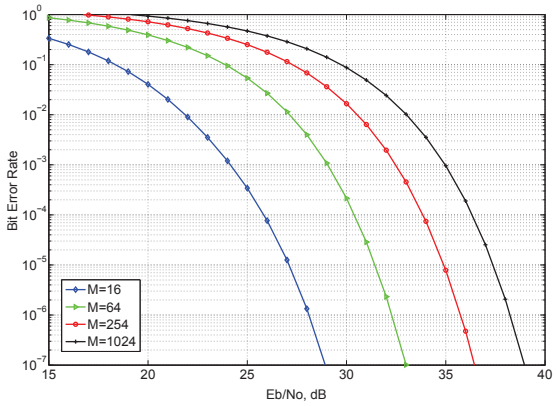


Figure 11. Performance of $M$PSK-CSK for odd values of $n$ ($M$ = 16, 64, 256, 1024).

## V. Conclusion

This paper proposes the design of constellations for $M$PSK-CSK for hybrid PLC-VLC cascaded systems. The aim is to design an efficient constellation for hybrid PLC-VLC cascaded systems. A mapping technique exploiting the HSV color space is used in PSK to CSK conversion. PSK and CSK are used over PLC and VLC channels respectively. The PSK-CSK conversion algorithm produces a distance $d_b$ that varies with the modulus of the PSK complex symbol, which is modulated by a correcting factor $\varepsilon$ to meet lighting and communication requirements. The optimization problem obtained is solved and the best distance between nearest symbols is $1.2619\sqrt{E_b}$ corresponding to $\mathbf{x} = \{0.133,\ 2.080,\ 7.372,\ 21.759,\ 60.867,\ 167.16,\ \ldots\}$. We then analyze performances of $M$PSK systems for $d_b = 1.2619\sqrt{E_b}$. For values of $M$ greater than 4, we give a general expression for odd and even values of $m$ separately, then we derive the probability in each case, and a general expression is proposed.

## References


[1] M. M. Rahman, C. S. Hong, S. Lee, J. Lee, M. A. Razzaque, and J. H. Kim, "Medium access control for power line communications: an overview of the IEEE 1901 and ITU-T G.hn standards," *IEEE Commun. Mag.*, vol. 49, no. 6, pp. 183–191, Jun. 2011.

[2] H. A. Latchman, S. Katar, L. Yonge, and S. Gavette, *IEEE 1901*. Wiley-IEEE Press, 2013. [Online]. Available: http://ieeexplore.ieee.org/xpl/articleDetails.jsp?arnumber=6645463

[3] S. Goldfisher and S. Tanabe, "IEEE 1901 Access System: An overview of its uniqueness and motivation," *IEEE Commun. Mag.*, vol. 48, no. 10, pp. 150–157, Oct. 2010.

[4] V. Oksman and S. Galli, "G.hn: The New ITU-T Home Networking Standard," *IEEE Commun. Mag.*, vol. 47, no. 10, pp. 138–145, Oct. 2009.

[5] "IEEE standard for local and metropolitan area networks–part 15.7: short-range wireless optical communication using visible light," *IEEE Std 802.15.7-2011*, pp. 1–309, Sep. 2011.

[6] R. J. Drost and B. M. Sadler, "Constellation design for channel precompensation in multi-wavelength visible light communications," *IEEE Trans. Commun.*, vol. 62, no. 6, pp. 1995–2005, Jun. 2014.

[7] R. Singh, T. O'Farrell, and J. P. R. David, "Performance evaluation of IEEE 802.15.7 CSK physical layer," in *Proc. IEEE GLOBECOM Workshops*, Atlanta, GA, USA, Dec. 9-13, 2013, pp. 1064–1069.

[8] E. Monteiro and S. Hranilovic, "Design and implementation of color-shift keying for visible light communications," *IEEE J. Lightw. Technol.*, vol. 32, no. 10, pp. 2053–2060, May 2014.

[9] S. Rajagopal, R. D. Roberts, and S. K. Lim, "IEEE 802.15.7 visible light communication: modulation schemes and dimming support," *IEEE Commun. Mag.*, vol. 50, no. 3, pp. 72–82, Mar. 2012.

[10] R. D. Roberts, S. Rajagopal, and S. K. Lim, "IEEE 802.15.7 physical layer summary," in *Proc. IEEE GLOBECOM Workshops*, Houston, TX, USA, Dec. 5-9, 2011, pp. 772–776.

[11] F. A. Farris, *Visualizing Complex-Valued Functions in the Plane*, AMC 10 1997.

[12] J. B. Conway, *Functions of One Complex Variable II*. Springer Science and Business Media, 1995, vol. 2.

[13] T. Komine and M. Nakagawa, "Integrated System of White LED Visible-Light Communication and Power-Line Communication," *IEEE Trans. Consum. Electron.*, vol. 49, no. 1, pp. 71–79, Feb. 2003.

[14] J. Song, W. Ding, F. Yang, H. Yang, B. Yu, and H. Zhang, "An Indoor Broadband Broadcasting System Based on PLC and VLC," *IEEE Trans. Broadcast.*, vol. 61, no. 2, pp. 299–308, Jun. 2015.

[15] W. Ding, F. Yang, H. Yang, J. Wang, X. Wang, X. Zhang, and J. Song, "A hybrid power line and visible light communication system for indoor hospital applications," *Comput. in Industry*, vol. 68, pp. 170–178, 2015.

[16] A. R. Ndjiongue, T. Shongwe, H. C. Ferreira, T. M. N. Ngatched, and A. J. H. Vinck, "Cascaded PLC-VLC Channel Using OFDM and CSK Techniques," in *Proc. IEEE GLOBECOM Conf.*, San Diego, CA, USA, Dec. 6-10, 2015, pp. 1–6.

[17] H. Ma, L. Lampe, and S. Hranilovic, "Integration of Indoor Visible Light and Power Line Communication Systems," in *Proc. 17th IEEE ISPLC Conf.*, Johannesburg, South Africa, Mar. 24-27, 2013, pp. 291–296.

[18] M. S. A. Mossaad, S. Hranilovic, and L. Lampe, "Amplify-and-Forward Integration of Power Line and Visible Light Communications," in *Proc. IEEE Global Conf. Signal and Inf. Process. (GlobalSIP)*, Orlando, FL, USA, Dec. 14-16, 2015, pp. 1322–1326.

[19] A. R. Ndjiongue, H. C. Ferreira, K. Ouahada, and A. J. H. Vinckz, "FLow-Complexity SOCPBFSK-OOK Interface Between PLC and VLC Channels for Low Data Rate Transmission Applications," in *Proc. 18th IEEE ISPLC Conf.*, Glasgow, Scotland, UK, Mar. 30-Apr. 2, 2014, pp. 226–231.

[20] A. D. Familua, A. R. Ndjiongue, K. Ogunyanda, L. Cheng, H. C. Ferreira, and T. G. Swart, "A Semi-Hidden Markov Modeling of a Low Complexity FSK-OOK in-House PLC and VLC Integration," in *Proc. 19th IEEE ISPLC Conf.*, Austin, TX, USA, Mar. 29-31, 2015, pp. 199–204.

[21] A. R. Ndjiongue, H. C. Ferreira, and T. Shongwe, "Inter-Building PLC-VLC Integration Based on PSK and CSK Techniques," in *Proc. 20th IEEE ISPLC Conf.*, Bottrop, Germany, Mar. 20-23, 2016, pp. 31–36.

[22] A. R. Ndjiongue, H. C. Ferreira, T. Shongwe, T. Ngatched, and A. J. Han Vinck, "PSK to CSK Mapping for Hybrid Systems Involving the Radio Frequency and the Visible Spectrum," *Telecommun. Syst.*, May 2016, Online First.

[23] A. R. Ndjiongue, T. Shongwe, and H. C. Ferreira, "Closed-Form BER expressions for HSV based MPSK-CSK Systems," *IEEE Commun. Lett.*, vol. PP, no. 99, pp. 1–1, 2017.